Accepted Manuscript

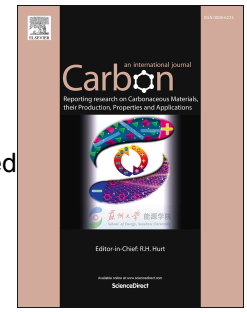

Particle size effect in porous film electrodes of ligand-modified graphene for enhanced supercapacitor performance

Gyoung Gug Jang, Bo Song, Kyoung-sik Moon, Ching-Ping Wong, Jong K. Keum, Michael Z. Hu

PII: S0008-6223(17)30383-4

DOI: 10.1016/j.carbon.2017.04.023

Reference: CARBON 11932

To appear in: *Carbon*

Received Date: 20 January 2017

Revised Date: 4 April 2017

Accepted Date: 15 April 2017

Please cite this article as: G.G. Jang, B. Song, K.-s. Moon, C.-P. Wong, J.K. Keum, M.Z. Hu, Particle size effect in porous film electrodes of ligand-modified graphene for enhanced supercapacitor performance, *Carbon* (2017), doi: 10.1016/j.carbon.2017.04.023.

Graphical Abstract

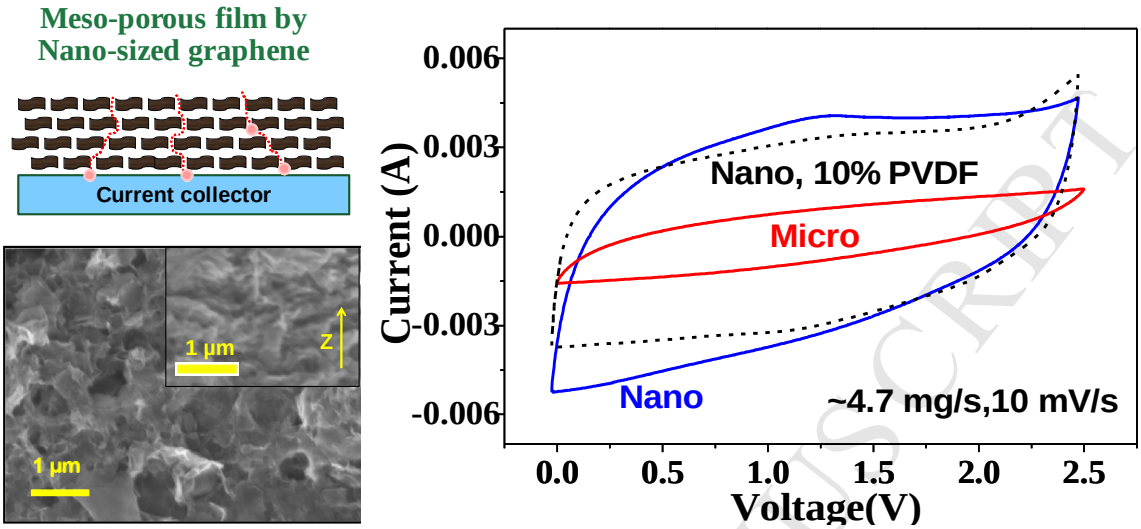

Particle Size Effect in Porous Film Electrodes of Ligand-Modified Graphene for Enhanced Supercapacitor Performance

Gyoung Gug Jang,[1#] Bo Song,[2] Kyoung-sik. Moon,[2] Ching-Ping Wong,[2] Jong K. Keum,[3] Michael Z. Hu[1#*]

[1] *Energy and Transportation Science Division, Oak Ridge National Laboratory (ORNL), Oak Ridge, TN 37831*
[2] *School of Material Science and Engineering, Georgia Institute of Technology, Atlanta, GA 30332*
[3] *Center for Nanophase Materials Sciences, ORNL*

[#]Authors of equal contribution.
[*]Corresponding author. Tel: 1-865-574-8782. E-mail: hum1@ornl.gov

ABSTRACT

Graphene-based electrodes for high performance supercapacitors are developed by taking advantage of particle size control, large mass loading, and surface functionalization of reduced graphene oxide (rGO) sheets. Two controlled sizes of graphene sheets (100-nm vs. 45-μm average lateral dimensions) were prepared to study two-electrode system performance. The nano-size graphenes led to the formation of mesoporous films, resulting in higher capacitance, better capactiance retension and lower equivalent series resistance (ESR), indicating better surface usability for diffusion and accessibility of electrolyte ions by shortening transport paths (compared with horizontally stacked films from micro-sized graphenes). For studies using an aqueous electrolyte, the maximum specific capacitance of nano-rGO film was 302 F/g (at 1 A/g with 4.3 mg/cm^2 of mass loading), which was ~2.4 times higher than micro-rGO film, and achieved a ~67 % reduced ESR. With an organic electrolyte, the nano-rGO delivered ~4.2 times higher capacitance (115 F/g at 2 A/g with 4.3 mg/cm^2), 4.0 times lower IR drops, and an order-of-magnitude lower charge-transfer resistance with an energy density of 18.7 Wh/kg. The results of this work indicate that the size control of graphene sheet particles for film deposit electroldes can be a simple but effective approach to improve supercapacitor performance.

KEYWORDS: nano sized graphene, graphene functionalization, reduced graphene oxide, supercapacitor

Introduction

Carbon based electrode materials have been considered very promising for energy storage devices because nanoporous carbons have relatively high electrical conductivity, large specific surface area and very practical benefits such as sustainablility, abundancy, and low to moderate cost resouce [1]. The porous carbons (e.g. activated carbon with high specific surface (1100~3000 m^2g^{-1})) generally increases capacitance with increased surface area [2]. In fact, a very large porosity of the activated carbons leads to low volumetric density and is unfavorable for high power and energy performance [2,2]. Particularly, pristine graphene could be an ideal carbon electrode material for high performance supercapacitors because of high theoretical specific surface area (up to 2630 m^2g^{-1}), fast electron mobility (e.g. mechanical exfoliation; > 2×10^5 $cm^2V^{-1}s^{-1}$), defined pore structure and good resistance to oxidative process [2,3].

Currently, liquid-phase exfoliated graphene (e.g. graphene oxide (GO)), despited of relatively low electron mobility (a layer of overlapping flakes; 1 $cm^2V^{-1}s^{-1}$) is considered to the most promising material for practical supercapactior device platform with available mass production [2]. Although many attempts have been made to use surface-unmodified GO to make conductive reduced graphene oxide (rGO) particle-based film electrodes, the irreversible graphene sheet restacking back to graphite during hydrothermal/chemical reduction results in the loss of usable surface areas and the graphene material properties such as unsatisfied conductivity. Various ligand molecules (also known as "spacers") have been introduced to spatially separate the rGO flake sheets for more effective ions diffusion between the two sheets [4,5,6,7,8,9]. Nevertheless, the structural advantage of functionalized rGOs, nanopore (<2nm), is often limited by some closed pores during conventionl electrode preparation, which engages horizontally packing of rGO flakes, plus the use of insulating polymer binders, conductive carbon agents in organic

solvents [7,10,11]. Also, the ligand functionalized rGOs usually have 0.8~1.5 nm of interlayer spacings (i.e. nanopores) [4,5,6,8,9]. They were still too small to access for large sized organic electrolytes (e.g. solvate tetraethylammonium (TEA) ion in acetronitrile is 1.3 nm) [1]. Also, the intrinsic horizontal stacking of graphene sheets leads to long path lengths of electrolyte ions diffusion and limitated contact points between active material (i.e., graphene film electrode) and current collector (i.e., stainless steel), resulting in slow ion and electron transporation [11,12]. Especially, the trasport kinetics of larger size organic and ionic electrolyte molecules are more hindered in these graphene based electrodes than aqueous electrolytes. To overcome the transport limitation, larger and shorter macro/mesoporous interspacing between the restacked sheet particles of ligand-grafted rGO were created via vertical alignment, N-dopoing, nano-template or holey graphenes [10,11,12,13,14,15,16].

In this work, we report the size effect of graphene particulates inside a porous film deposit (as electrode) on a carbon fiber paper (CFP, as current collector for supercapacitor). The films were deposited by drop-casting the slurry of molecular ligand grafted rGO dispersed in ethanol. The surfaces of nano-sized graphene oxide (GO) flake sheets were first functionalized by adding 2,5-diamino-1,4-dihydroxylbenzene dihydrochloride (DDDC) molecular ligands, and then chemically reduced to form the nano-DDDC-rGO. The slurry of nano-DDDC-rGO with/without polymer binder were then deposited on the CFP. One major finding based on XRD studies is that the DDDC ligand functionalized rGO shows a particle size-dependent crystalline structures in film deposits. Ligands enable the increased interspacing between rGO sheet in relative to the one for restacked rGO. Micron-sized DDDC-rGO, as a baseline material, form a horizontally packed "dense" film that contains crystallized stacking structure although the molecular interspacing is

preserved. In contrast, deposition of smaller sized nano-DDDC-rGO sheets produce mesoporous films (10~50 nm) that prevent formation of graphitization stacking domains.

We have also studied the loading amount effect on capacitance and kinetic performance for both nano-sized (~100 nm) and micron-sized (~45 µm) DDDC-rGO sheets particulate deposit films. Most high performance rGO based supercapacitor studies were performed with a low loading amounts (0.1~1.0 mg/cm^2) [4,5,6,7,9,17,18]. Note that similar to carbon based electrodes, specific capacitance of micron-sized film electrode decreased with increasing the loading amount. However, for the nano-DDDC-rGO film electrodes we have found that their specific capacitance increased with increasing graphene loading amount. Both aqueous electrolyte and organic electrolyte were studied to evaluate the nano-size graphene based supercapacitor cell performance. The nano-size graphene derived microstructure in the deposit film electrode have led to higher specific capacitance, faster kinetics and better contact of active material/current collector, compared with the micron-sized graphene film deposit.

2. Experimental

All the chemical reagents in this work were commercially available and used as received. GO was synthesized from natural graphite powders (Asbury 230U (~40-50 µm in size) and nano-graphite Nano 307 (<100 nm, SS 350 m^2/g) from Asbury Carbons, PA) by a modified Hummers method [19]. Carbon fiber paper (CFP, Spectracarb 2050A - 1050) was purchased from FuelCellsEtc (College Station, TX).

2.1. Synthesis of ligand-grafted graphene (DDDC-rGO)

GO slurry contains 120 mg of GO solid sheet/flake particles in 40 mL of 200-proof ethanol and was sonicated for 2 hrs to homogenize. 52 µl HCl was added into the slurry and also mixed with

150 mg 2,5-Diamino-1,4-dihydroxylbenzene dihydrochloride (DDDC) in a reaction vessel sealed with a cap. The reaction mixture was allowed to react at 120 °C in an oven overnight for 16 hrs. Then the reacted slurry was cooled down to room temperature. Then, the slurry was directly reduced by hydrazine. For chemical reduction of GO or the DDDC ligand composite GO, 0.436 ml NH_3 (7 N in methanol, Sigma-Aldrich) and 35.9 µl $N_2H_4{\cdot}H_2O$ (99+%, Alfa Aesar) was dropped into the reaction vessel and the mixture was held at 95 °C for 3 hrs. After cooling down to room temperature, the slurry was transferred into centrifuge bottles and centrifuged for 10 min at 12,000 rpm. Supernatant was decanted. The ethanol and water (~50 mL) washing and centrifugation were repeated 6 times to wash out the residual un-reacted DDDC (indicated by a purple color). Micro-DDDC-rGO and nano-DDDC-rGO are prepared from Asbury 230U and Nano307 graphite powder, respectively.

2.2. Graphene film deposition onto CFP discs

The above harvested DDDC-rGOs (nano and micro) was re-dispersed in ethanol with sonication for 1 hr to form a homogeneous suspension slurry (~5 g/L). At the beginning of deposition, the porous CFP was drained out some graphene slurry. A continuous graphene film formed on the surface of the CFP via continuous deposition. Once a continuous thin film formed on the porous CFP, the permeate rate of graphene solution was slow down and the film was mainly formed by solvent drying. The drop-casting deposition was repeated to achieve a desirable mass (1~6 mg). PVDF bound DDDC-rGO slurry was prepared by mixing 90 wt% DDDC-rGO in ethanol and 10 wt% PVDF in N-methyl-2-prrolidone (NMP) solution. Then, add more NMP to adjust 1:1 of ethanol and NMP solution containing ~5 g/L of graphene slurry. The slurry was drop casted on the CFP at 80°C.

2.3. Materials Characterization

Scanning electron microscopy (SEM) imaging was carried out on a field emission scanning electron microanalyzer (Merlin, Carl Zeiss AG). X-ray diffraction (XRD) measurements were conducted using a PANalytical X'Pert Pro MPD equipped with an X'Celerator solid-state detector, using X-rays generated at 45 kV/40 mA, and X-ray beam wavelength was λ=1.5406 Å (Cu Kα radiation). Surface chemistry data were obtained using X-ray photoelectron spectroscopy (XPS, K-Alpha XPS system, Thermo Fisher Scientific) equipped with a mono-chromated Al-Ka source (hv 1⁄4 1486.6 eV). The 180 double focusing hemispherical analyzer with 128-channels was operated at a constant pass energy of 200 eV for survey spectra and 50 eV for core level spectra. Peak fitting was performed using the Avantage program (v4.61). Spin–orbit doublets were related using the appropriate area and separation relationships after applying a Shirley background correction. Electrical resistivity of deposited film (<0.5 mg/cm^2) were measured by four-point probe set-ups.

2.4. Electrochemical Performance Measurement

A pair of identical graphene film deposits on two CFP discs were assembled into a prototype supercapacitor (in the form of coin cells or split cells) for measuring the electrochemical performance. Aqueous electrolyte solution (1 M H_2SO_4) or an organic electrolyte solution (1 M Tetraethylammonium tetrafluoroborate (TEA) in acetonitrile (AN)) and a pair of DDDC-rGOs film deposits on CFP circular discs were assembled in a symmetrical two-electrode configuration following a previously reported procedure [4]. Cyclic voltammetry and galvanostatic charge/discharge measurements were obtained over the potential range of 0 to 0.8 V for split cells (using aqueous electrolyte) and 0 to 2.5 V for coin cells (using organic electrolyte). Measurements were carried out with a Versastat 2-channel system (Princeton Applied Research). A *specific capacitance* is calculated by using the integrated area of the CV curve by [4,6]:

$$C_{sp} = \frac{Q}{\mu \times m \times \Delta V} \times 2$$

Where Q is the integrated area of the CV curve, m is the total mass of the deposited graphene active material (g) on a pair of CFP discs, μ is the scanning rate (V/s), and ΔV is the potential window of discharge. The *gravimetric capacitance* was also calculated from the galvanostatic charge/discharge curves with current density using the formula (for a pair of electrode thin film configuration) [4,6]:

$$C_{sp} = \frac{i \times \Delta t}{\Delta V} \times 4$$

Where i(A) is the discharge current, Δt(s) is the discharge time, ΔV(V) is the voltage change (excluding the IR drop) within the discharge time, the multiplier of 4 adjust the capacitance of the cell and the combined mass of two electrodes to the capacitance and mass of a single electrode. The *energy density* (E) and *power density* (P) in the Ragone plots were calculated using the following equations [4,6,8,9,16]:

$$E = \frac{1}{8} C_{sp} V_{max}^2$$

$$P = \frac{E}{\Delta t}$$

Where C_{sp} is the specific capacitance, V_{max} is the potential window obtained from the discharge curve subtracted by the V_{drop} (i.e. excluding IR drop) and Δt is the time for complete discharge.

3. Results and discussion

The ligand modification generally improves not only the wettability of the graphene surface for uniform deposit electrode film, but also the charge storage capability [20]. In this work, the ligand molecule DDDC was used to modify graphene mateirals to prevent the

restacking of graphene sheets and increase intercalation spacing between restacked graphene sheets.

The DDDC composition onto graphene in our samples (labled as micro-DDDC-rGO and nano-DDDC-rGO) was confirmed by XPS. Fig. 1 shows the C 1s XPS spectra of a referential micro-rGO consists of five peaks from C=C (sp^2), C-C(sp^3), C-N, C-O and O=C-O. After DDDC functionalization and reduction of the GO materials, the peak intensity of the sp^2 carbon decreased remarkably, while other peaks increased significantly. Note that the peak from C-N in micro-DDDC-rGO increased significantly. The N amount (i.e. amine, 3.6 atomic %) in DDDC-rGO sample was 2.6 times higher than the ligand-free rGO sample (1.4%). The total atomic ratios in the samples, calculated from semi-quantitative analysis of the XPS data are shown in Supplementary Table S1. It supported the existence of the pyridine-like N from the introduced heterocyclic group in micro-DDDC-rGO. The nitrogen existence in rGO sample was associated with hydrazine reduction. The nano-DDDC-rGO sample also showed these similar XPS features (e.g. sp^2 peak decrease and N amount increase).

Traditionally, drop casting of GO or rGO slurry of micron sized particles onto a substrate tend to form a dried film containing microstructure of dense horizontally stacked graphene sheets. In contrast, our nano-DDDC-rGO film deposits contains a non-stacked porous film structure, which may enhance transport pathways for electrolyte ions and surface usability. Fig. 2c and 2d shows the SEM morphological comparison of nano- and micro-DDDC-rGO film deposits on the CFP substrate. The 100 nm nano-sized graphene sheets formed rough and porous surface morphology, while 45 µm micro-sized graphene deposits form a relatively smooth surface of a continuous stacked films after fully dried. The cross sectional SEM image of nano-DDDC-rGO film (Inset Fig. 2c) clearly shows mesoporous structure (10~50 nm) without any aggregated

particles or horizontally stacked layers. On the other hand, the micro-DDDC-rGO film deposit (Fig. 2d and inset) shows a dense horizontally stacked structure. In principle, the close restacking of lamellar film structure retards diffusion of electrolyte ions due to long path lengths resulting in a relatively slow kinetic response [11]. However, the open mesopores formed by non-stacked nano-sheets/particles could offer a microstructure to reduce the diffusion length of electrolyte ions through the graphene film deposit layer to reach the current collector. This is illustrated by the schematic (Fig. 2a&b).

The crystalline structures of nano-DDDC-rGO, micro-DDDC-rGO, and their referential GO film deposit samples were characterized by XRD (Fig. 3). The XRD peaks of the GO film corresponds to the interlayer distance of re-stacked GO sheet particles, resulting from intercalated water molecules and the surface oxygen-containing functional groups. Composite with additional ligand molecules on GO particle surfaces increases the interlayer distance, indicated by the shift of XRD diffraction to small angles (at two theta position of 4.5-8°, [001]) from GO (at 10-11°, [001]) or disappearance of [001] crystalline peak [4,5,6,7]. The 45 μm sized GO ("micro-GO") slurry deposits exhibit a peak at 2θ=11.2°, [001], corresponding to an average interlayer distance of 0.730 nm. Upon chemical reduction, the loss of oxygen groups occurs, and rGO become restacked, resulting in reduced interlayer spacing (24.0°, 0.370 nm). After DDDC ligand functionalization on GO sheets and its following reduction, the resulted material ("micro-DDDC-rGO") shows two broad peaks at 2θ= 11.0° (0.803 nm) and 24.3° (0.366 nm) at [002] direction (the moderately aligned graphitic arrays). The "nano-GO" has a broad [001] peak at 2θ=11.1° (0.796 nm), which is essentially the same structure as "micro-GO" deposit material. However, upon chemical reduction, the [001] nano-GO peak disappeared. After DDDC composition and following reduction, the [001] GO peak also disappeared in the "nano-DDDC-

rGO". The XRD data indicate that the film deposit of "nano-DDDC-rGO" may exist as one and a few layers rGO sheets without the crystallized re-stacking as for nano-GO.

DDDC composite renders hydrophilicity of the graphene surface, resulting in a uniform film in micro scale. Generally, simply reduced GO is problematic to form a uniform thin film due to agglomeration and surface hydrophobicity of rGO, resulting in precipitation in an aqueous solvent. Drop casting deposit of micro- and nano-rGO forms a rough and cracked film. Specifically, binder free micro- and nano-rGO deposit films with > 2.5 mg/cm^2 of mass loading on current collector were not properly prepared as a uniform thin film, because of severe cracking and peeled-off via strong aggregation (Supplementary Fig. S1). However, nano- and micro-DDDC-rGO enable to form uniform micro-scale thin film deposits up to > 6.0 mg/cm^2. We measured BET surface area of nano-DDDC-rGO and micro-DDDC-rGO electrode films on CFP substrates. The measurable surface area of DDDC-rGOs films were very low (< 1 m^2/g) due to organic molecule inhibition to nitrogen adsorption on the surfaces [20].

In order to assess the "size effect" of graphene sheet particles on electrochemical performance, we have evaluated the film deposits of nano-DDDC-rGO, compared with the performance data measured for micro-DDDC-rGO. The prototype split/coin cell performance tests were conducted under galvanostatic mode both in the potential range of 0-0.8Vs with an aqueous electrolyte and the range of 0-2.5V with an organic electrolyte. DDDC ligand composite rGO showed an enhanced capacitance due to increased interlayer spacing and surface wettability resulting in increased graphene surface accessibility of electrolyte, compared with rGO [20]. Fig. 4a shows the CV curves for both nano-DDDC-rGO (deposit loading amount; ~4.4 mg/cm^2) and micro-DDDC-rGO (~4.3 mg/cm^2 loading) electrodes measured at the same scan rate at 10 mV/s. First, with the aqueous electrolyte (e.g. 1M H_2SO_4) and nearly same loading of graphene active

materials, the gravimetric capacitance value for nano-DDDC-rGO (i.e., the integrated CV curve area at 10 mV/s) was larger than the one for micro-DDDC-rGO. The specific capacitance for nano-DDDC-rGO cell was 255 F/g which is ~2.4 times higher than 107 F/g for micro-DDDC-rGO cell. Fig. 4b shows the galvanostatic charge/discharge plots in the potential range (0-0.8V) for nano and micro-DDDC-rGO with the same loading amount at a low current density of 1 A/g. The charge and discharge curve of nano-DDDC-rGO electrode exhibits ~3.1 time longer than micro-DDDC-rGO. The data resulted in 302 F/g for nano-DDDC-rGO cell, which is ~2.7 times higher than 113 F/g of micro-DDDC-rGO cell.

Also, the specific capacitance enhancement via size control was evaluated with varying deposit loading amount of the graphene active materials (Fig. 4c). We observed that specific capacitance of micro-DDDC-rGO films decreased with loading amount (Fig. 4c), which is consistent with the trend reported in literature for other carbon-based supercapacitor cells [11]. It can be explained that the thicker graphene deposit films with horizontally stacking structure tend to reduce the accessibility of particle surfaces within the film deposit and increase the path length for ion transport across the graphene electrode film, resulting in loss of capacitance and other kinetic performance. In contrast, we have discovered that nano-DDDC-rGO films exhibited a different loading effect for the aqueous electrolyte. The smallest loading amount (1.2 mg/cm^2) has lower capacitance value of 171 F/g @ 10 mV/s (177 F/g @ 1 A/g) for a nano-DDDC-rGO cell than for a micro-DDDC-rGO cell (251 F/g). The lower capacitance of nano-DDDC-rGO relative to micro-DDDC-rGO could be explained by electrical resistivity of deposit film (Supplementary Table S2). Electrical resistivity of nano-DDDC-rGO is higher than micro-DDDC-rGO at low loading. However, the benefit of low resistative micro-DDDC-rGO electrode may decrease by increasing length of ion path way and restacking with increasing film loading

amount. As the loading amount was increased to ~4.3 mg/cm^2, the specific capacitance of nano-DDDC-rGO cell increased to 302 F/g. Note that this is a promising feature that we may take advantage to tailor and improve the absolute energy and power of a supercapacitor device.

Besides the impact on capacitance values, the nano-DDDC-rGO films have exhibited higher electron/ion transport performance, compared to the baseline micro-DDDC-rGO films. Figure 4b shows that the voltage (*IR*) drop for the nano-DDDC-rGO is 0.08V, which is smaller than 0.21V for the micron-DDDC-rGO. The smaller IR drop indicates that the capacitive reversibility is high, attributed by the high-quality contact at the interface of active layer/current collector [12]. On the other hand, the IR drop values for both nano and micro-DDDC-rGO increased in proportional to the loading amount. Furthermore, comparing with asymmetric charging/discharge curve for micro-DDDC-rGO, the one for nano-DDDC-rGO were more symmetric, indicating the capacitive reversibility was high, consistent with its electrochemical characteristics.

Nyquist plot, as shown in Fig. 4d, indicates that the slopes for nano-DDDC-rGO electrode was higher in the low frequency region than the slope for the micro-DDDC-rGO, suggesting higher ion diffusion behavior due to the short path way of electrolyte in the nano-electrode. The first and second intersects of semicircle curve in the high frequency region of the Nyquist plot implies the equivalent series resistance (ESR; R_s) and charge transfer resistance (R_{ct}), respectively. As the reference, micro-DDDC-rGO shows R_s of 1.5 Ω and R_{ct} of 4.0 Ω while the nano-DDDC-rGO showed lower R_s of 0.5 Ω and R_{ct} of 2.7 Ω at the same medium loading amount. The low R_s and R_{ct} implies an improved electrical conductivity and fast electrochemical reaction at the interface between electrode and electrolyte, respectively. ESR is an important practical factor for high performance supercapacitor. The similar features of higher ion diffusion

and lower ESR of nano-DDDC-rGO were also observed with increase of loading amount (Fig. 4e).

Fig. 4f shows the capacitance retention (with respect to 5 mV/s) with increasing scan rates. Capacitance usually is associated with surface usability. At low scanning rate, electrode have the highest capacitance and best electrochemical reactivity due to full usage of the entire electrode. However, at higher scanning rate, the ion mobility and electrode surface usability generally decreases due to preferential ion diffusion to minimum distance in electrode, resulting in decrease of capacitance [4,5,6,7]. The nano-DDDC-rGO material has effectively improvement of the capacitance retention at high scan rates, compared with micro-DDDC-rGO. The relative retention efficiency of nano-DDDC-rGO is better at low and high loading. We believe the well distributed nano-pores in nano-DDDC-rGO film have more porous structures with short ion paths than micro-DDDC-rGO. It resulting in enhanced surface usability at high scan rates.

It is no surprise that acid-based aqueous electrolyte showed a higher conductivity (up to ~1 S/cm) than for the organic electrolyte (e.g. TEA-AN), thus, providing the split cell device a higher power. However, due to the narrow electrochemical stability window (1.23 V) of water, the operating voltage is relatively low (~1V) [1]. Thus, the possible energy storage in the aqueous electrolyte supercapacitors is limited. Organic electrolytes have a wider electrochemical stability window (2.7 - 2.8 V) compared to aqueous electrolytes [1]. Even though their lower ionic conductivity and specific capacitance relative to aqueous electrolytes, the high cell voltage allows organic electrolyte supercapacitors to deliver a higher specific energy than aqueous system. Here in this work the coin cell performances using an organic electrolyte (1M TEA -AN) were evaluated for nano- and micro-DDDC-rGO materials. Out data (Fig. 5) shows that nano-DDDC-rGO electrode exhibited much higher cell performance, compared to the micro-DDDC-

rGO electrode. At the large mass loading of ~4.7 mg/cm^2, the gravimetric capacitance value of nano-DDDC-rGO (blue solid line, w/o binder, 109 F/g @ 10 mV/s) was 4.2 times higher than the one for micro-DDDC-rGO (red solid line, 26 F/g) (Fig. 5a). The PVDF binder (i.e. 10% PVDF bound on nano-DDDC-rGO; black dot line) did not show significant capacitance loss.

For the charge and discharge curve with the organic electrolyte, nano-DDDC-rGO electrode exhibits ~23 time longer than micro-DDDC-rGO in the potential range of 0-2.5V (Fig. 5b). The data results in a capacitance value of 117 F/g (at 0.5 A/g), which is ~13 times higher than the value of 9 F/g for micro-DDDC-rGO. The PVDF bound nano-rGO (i.e. nano, 10% PVDF) did not show significant capacitance loss. The large electrolyte ions (i.e. 1.3 nm) are spatially hindered to access into the densely stacked interlayers (~0.730 nm) of the micro-DDDC-rGO film electrode and thus, the ion mobility of the electrolyte is reduced, leading to the poor capacitance and charge-discharge kinetics. Even at higher current density (i.e. 1-2 A/g), micro-DDDC-rGO did not provide available values. Also, Fig. 5c shows the loading effect of nano-DDDC-rGO on specific capacitance. The small loading amount (2.1 mg/cm^2) has the highest capacitance value of 173 F/g @ 10 mV/s. The porous nano-DDDC-rGO film deposit has little crystalline-type stacked layers/domains, resulting in more graphene surface accessibility and thus higher capacitance. As increase the loading, the capacitance of nano-DDDC-rGO decrease and stabilized to 90-110 F/g. This trend seems to be different from the case for aqueous electrolyte (discussed above). This is probably because some domains of porous nanostructures in the nano-DDDC-rGO has certain difficulty to allow access and transport of organic electrolyte. The more loading/thickness of such materials may not enable to favor the proportional gain in capacitance and kinetic performance, rather it reduces the specific capacitance.

In terms of electron/ion transport for organic electrolyte in graphene film electrode, the nano-DDDC-rGO exhibited much better performance in organic electrolyte, compared to micro-DDDC-rGO. Fig. 5b showed that the voltage (IR) drop of the nano-DDDC-rGO was 0.38 V which is lower than 1.47 V of the micron-DDDC-rGO. Note that PVDF bound nano-DDDC-rGO exhibited 0.12V of IR drop. The polymer addition improves the quality of contact at the interface of active layer/current collector and more symmetric charge/discharge curve, leading to ideal capacitor.

Nyquist plot for the organic electrolyte-based coin cells, as shown in Figure 5d, indicate that the higher slopes of nano-DDDC-rGO in the low frequency region clearly show higher ion diffusion behavior, due to the short path way of electrolyte. The both ESR of nano-DDDC-rGO and micro-DDDC-rGO are a similar values of ~3.6 Ω. However, the fitted values of R_{ct} for nano-DDDC-rGO is 11.9 Ω, which is 10 times smaller than of micro-DDDC-rGO (118 Ω). The PVDF bound nano-DDDC-rGO is 5.0 Ω. The dependence of the phase angle on frequency (Bode phase plot) for nano- and micron-DDDC-rGO is shown in Fig. 5e. The impedance phase angle plots show capacitive behavior at low frequency and inductive behavior at high frequency [21, 22]. At the same loading, the characteristic frequency, f_0, of nano-DDDC for phase angle of 45° (the equal point for the resistive and capacitive impedances) is 0.034 Hz (corresponding elapsed time; 29.4 s) which is higher than 0.00 Hz of 0 kV (>100s). The PVDF bound nano-DDDC-rGO is 0.066 Hz (15.2 s). The rapid frequency response suggests that the size effect of nano-DDDC-rGO enhance the electrolyte ion transport rate. For inductive behavior, nano-DDDC show a similar capacitor-to-inductor transition of carbon based supercapacitor (e.g. activated carbon) as the frequency increase [22]. In contrast, the higher phase angle of micro-DDDC-rGO at high frequency may be attributed to electrode porosity difference [22].

Fig. 5f shows the capacitance retention (with respect to 10 mV/s) of organic electrolyte coin cells with increasing scan rates. The nano-DDDC-rGO effectively improve the capacitance retention with increasing scan rates, compared with micro-DDDC-rGO. The relative retention efficiency of nano-DDDC-rGO is more improved by addition of PVDF. For PVDF bound nano-DDDC-rGO, the temperature effect was evaluated. At 65 °C, capacitance retention efficiency improves as increase of scan rates. As discussed in case of an aqueous electrolyte, the ion mobility in nano-DDDC-rGO film structure was faster than micro-DDDC-rGO film structure. Also, the PVDF binding improve the cell kinetic performance with no loss of capacitance.

The cycling stability is one of the most important tests for practical supercapacitor. Micro-DDDC-rGO electrode in aqueous electrolyte split cells had a capacitance retention of ~90 % after 8,000 cycle [20]. Thus, the cycling stability nano-DDDC-rGO in aqueous and organic electrolyte was tested by galvanostatic charge-discharge at different current density. For aqueous electrolyte, nano-DDDC-rGO exhibited capacitance retention of 100% after 3000 cycles for 1 A/g [Inset of Fig. 6]. When measured at 2 A/g, the capacitance dramatically dropped to 82% and gradually increased around 1000 cycle, then decreased to 130% of the initial value, which might be associated with certain activation process such as surface wetting and electrolyte intercalation between the graphene layers. After 6000 cycles and relaxation for overnight, the cell recovered the capacitance to 150% and decreased during 8000 cycles. For more 2000 cycles to 10,000 cycles, the similar capacitance recovery was observed but the capacitance retention dropped. The similar activation behaviors were often observed in metal oxide composite graphene and ligand modified graphene electrode with aqueous electrolyte [7,10,14], but requires further characterization for complete understanding. For organic electrolyte coin cells, the capacitance of binder free nano-DDDC-rGO drop for 200 cycles and stabilized to 60% of retention after

3000 cycles. Addition of PVDF binder significantly improve the cycling stability. The early capacitance drop was reduced and the retention was stabilized to 74% after 6000 cycles. We found the cell performance of nano-DDDC was varied by dispersion solvents, binder and electrolytes. Optimization of cell performance needs to be studied in the future.

The *Ragone plot* shows the energy density and power density of our nano-DDDC-rGO supercapacitor cells with mass loadings of 1.0~6.0 mg/cm^2 in the aqueous and organic electrolytes (determined from the galvanostatic discharge curves). For our aqueous electrolyte split cells, the energy density values are in the range of 4.0~6.4 Wh kg^{-1} at a power density range of 0.7~0.2 kW kg^{-1} which are comparable with the recently reported high performance rGO based supercapacitors (i.e. Electrostatic double-layer capacitance). For our organic electrolyte coin cells, the achieved maximum energy density of 29.3 Wh kg^{-1} at power density of 1.1 kW kg^{-1} is beyond the reported values in the literature. The information of reported values is available in supporting information (Supplementary Table S3). This indicates a great potential of the proposed nano-sized, ligand-functionalized, and binder-tailored composite film electrodes for high-performance supercapacitors. A multi-variable study such as polymer binders, organic and ionic electrolyte will be valuable in the future to optimize electrode/electrolyte material combination and processing conditions for energy storage.

4. Conclusions

In this study, we successfully demonstrated a new class of high capacitive graphene-ligand-binder composite film electrodes for supercapacitors by simply controlling graphene sheet particle size (from 45-µm down to 100 nm), following appropriate DDDC ligand functionalization and binder formulation. This novel nano-DDDC-rGO approach enables the

transformation from traditional rGO-based electrodes to a new generation of nanocomposite electrodes that can achieve highly interconnected porous microstructures by preventing serious problem of traditional re-stacking of rGO sheets. Compared to the large micro-sized DDDC-rGO electrode (baseline), nano-DDDC-rGO electrodes (at high mass loading) have shown significantly higher capacitance and kinetic performance. Especially, for large molecular organic electrolyte, the nano-DDDC-rGO electrode could impart remarkable capacitance and high energy density because of a synergetic effect between the interconnected macro/mesopores (with minimized existence of non-stacked sheet layers/domains in the film deposits), which are able to create facile ion/electron transport pathways for electrolyte. Moreover, the overall energy density achieved with our nano-DDDC-rGO electrode in combination with organic electrolyte are higher than the high-end supercapacitors. The nanocomposite graphene film electrode design route reported here is simple and effective for large-scale production and is thus expected to be readily applicable to energy storage devices requiring both high power and energy density, such as mobile electronic devices and electric vehicles.

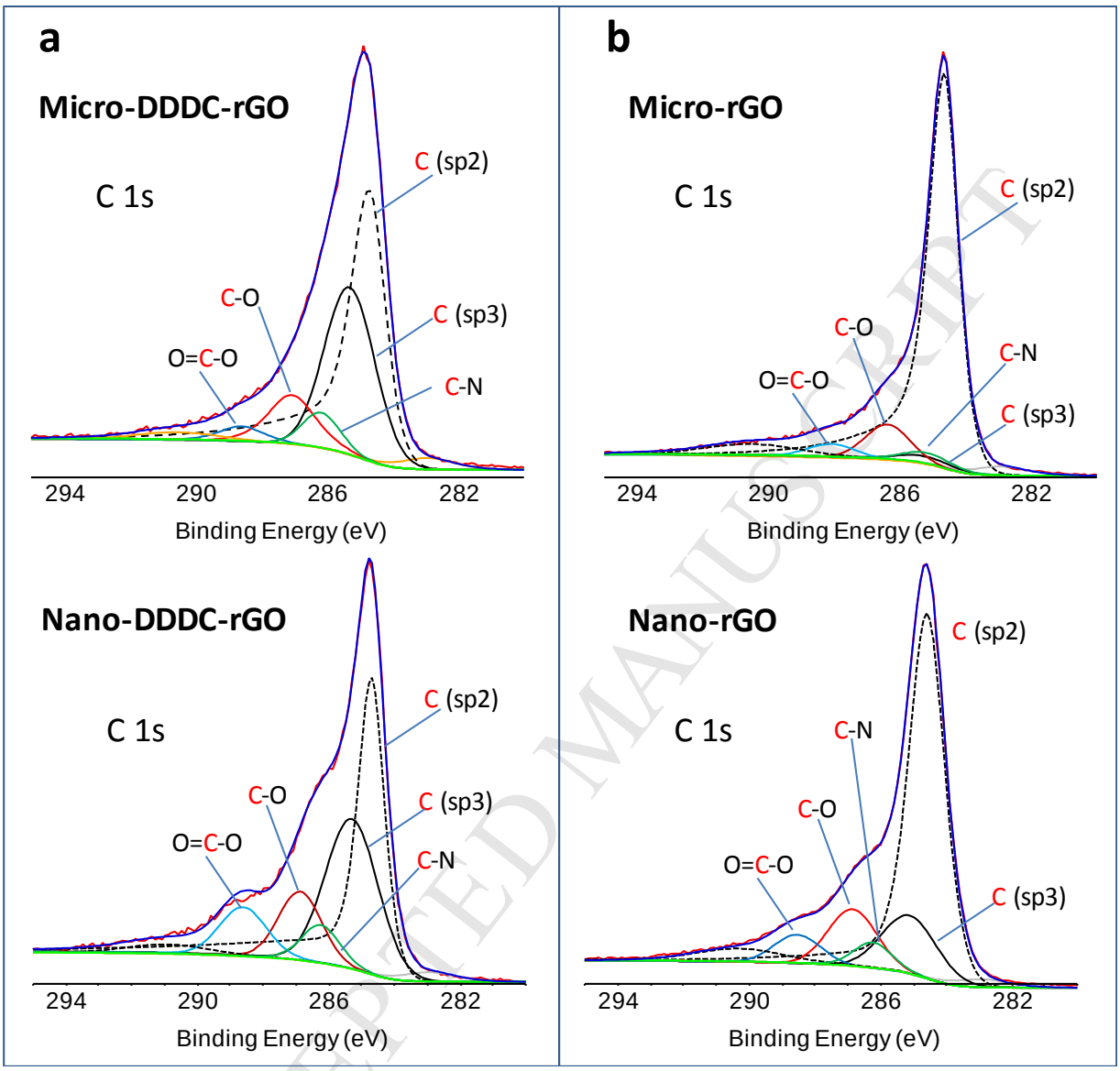

Fig. 1. XPS patterns of a) Micro-DDDC-GO and nano-DDDC-rGO, b) Micro-rGO and nano-rGO films

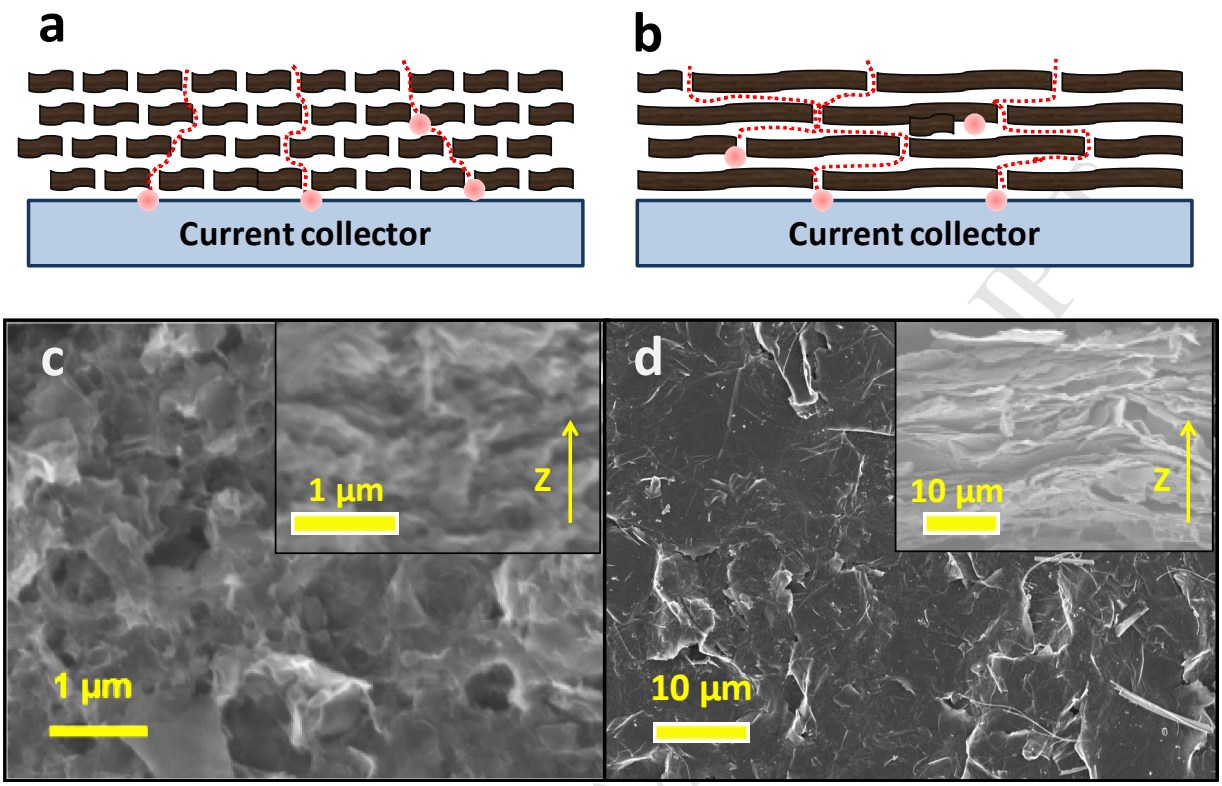

Fig. 2. Schematic illustration of ion diffusion direction based on the morphologies of two functionalized rGO electrodes (nano-DDDC-rGO and micro-DDDC-rGO) (a) Electrolyte ions were homogeneously and directly diffused in nano-porous sheets. (b) Electrolyte ions diffused in long pathway because of the horizontally stacked sheets. SEM images showing particle size-dependent morphology of deposited films of DDDC-rGOs. (c) Top surface view of porous nano-DDDC-rGO. Inset is the cross section SEM image of the deposit film. Z is a vertical direction means in perpendicular to the film surface. (d) Top surface view of densely-stacked micro-DDDC-rGO. Inset is the cross section SEM image of the deposit film.

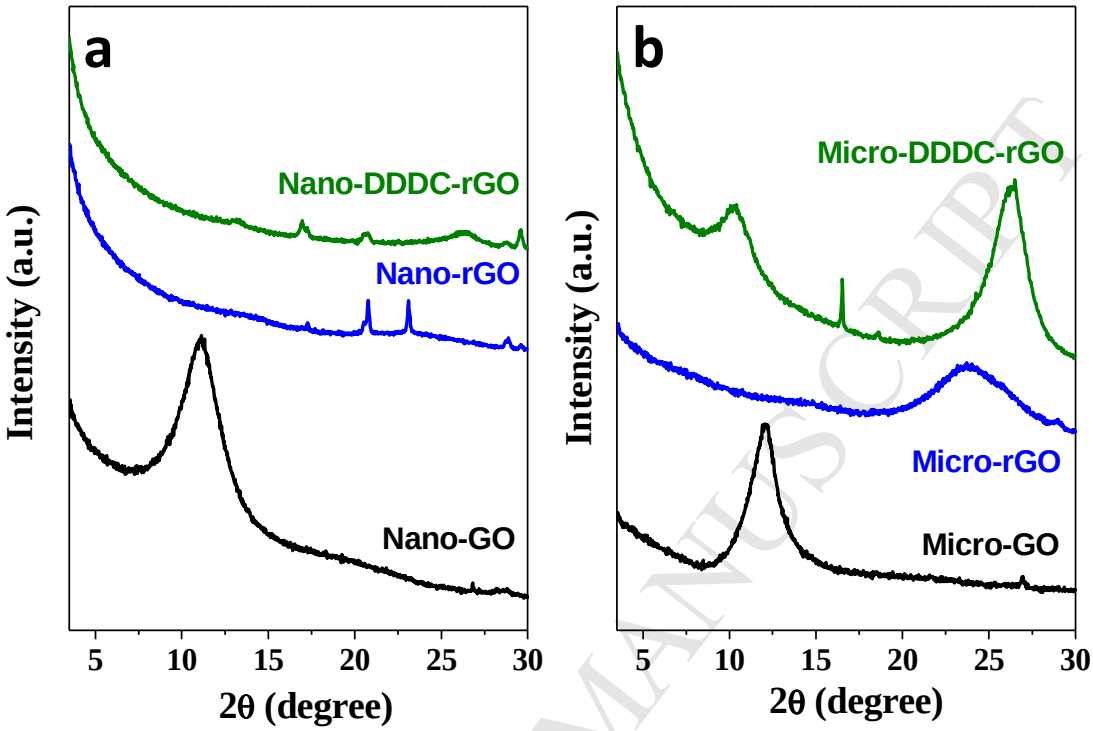

Fig. 3. X-Ray diffraction patterns of a) nano-GO, nano-rGO and nano-DDDC-rGO, b) micro-GO, micro-rGO, micro-DDDC-rGO films

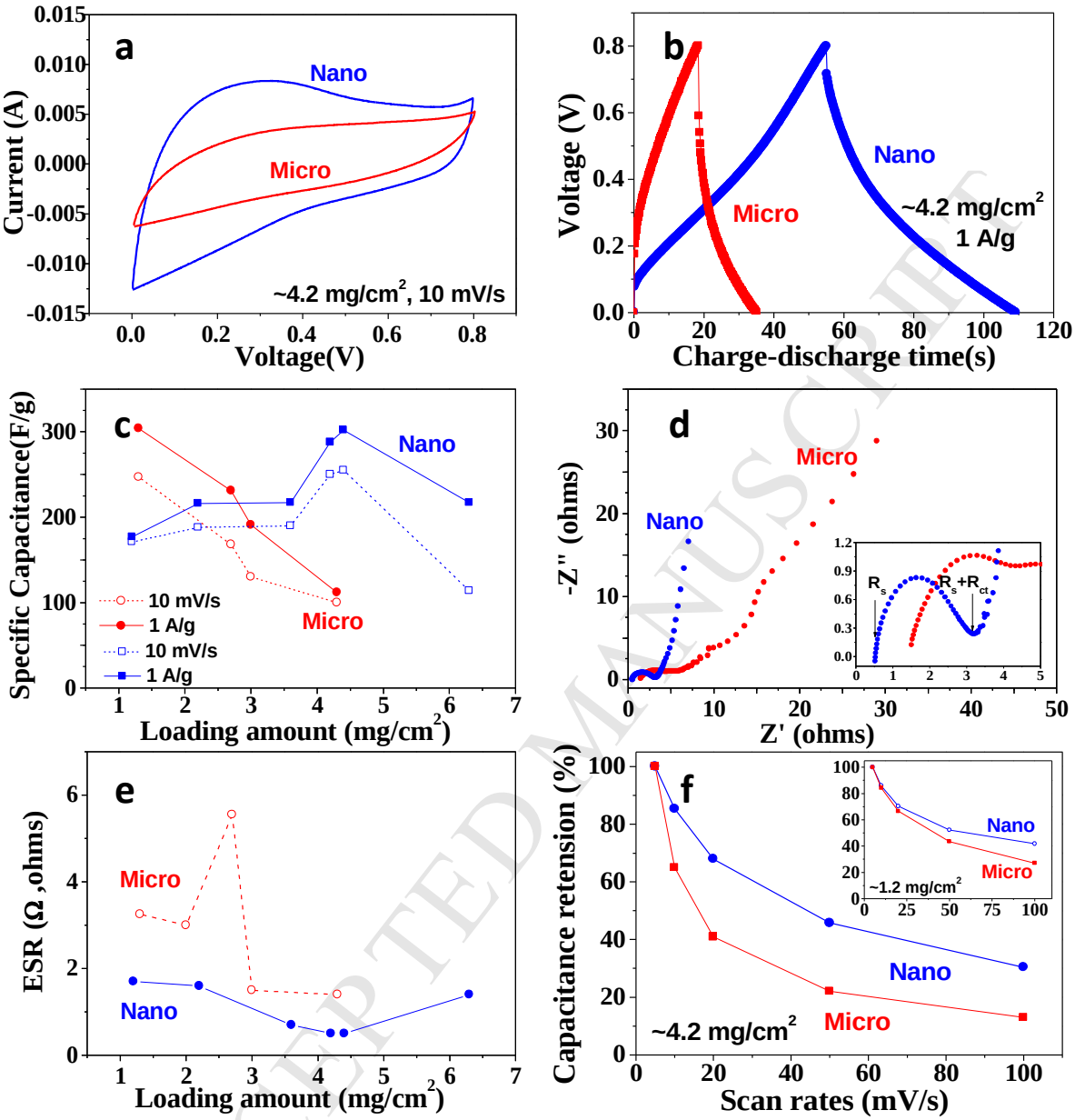

Fig. 4. Aqueous electrolyte supercapacitor split cell performance of nano-DDDC-rGO versus micro-DDDC-rGO film in a two-electrode system with 1M H_2SO_4. (a) CV curves at a scan rate of 10 mV s^{-1};(b) Galvanostatic charge/discharge curves at a current density of 1 A/g; (c) Specific capacitance comparison as function of deposit loading amount; (d) Nyquist plot. Inset is a high frequency region; (e) ESR comparison; (f) Relative specific capacitance retention as function of scan rates. Inset is a low loaded electrode.

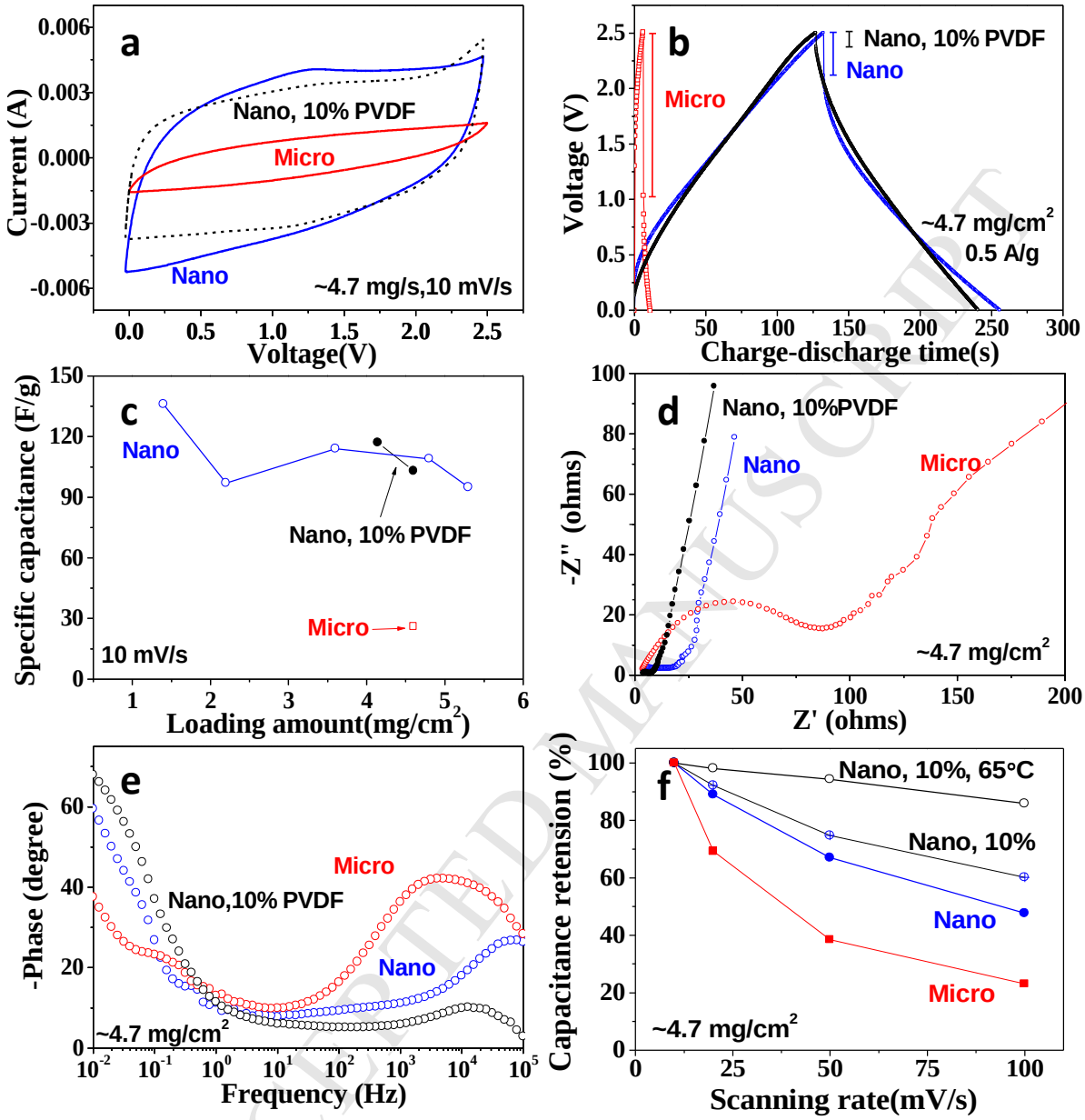

Fig. 5. Organic electrolyte supercapacitor coin cell performance of nano-DDDC-rGO (blue ; w/o binder, black : 10% PVDF binder) versus micro-DDDC-rGO film(red: w/o binder) in a two electrode system with 1M TEA in AN. (a) CV curves at a scan rate of 10 mV s^{-1}; (b) Galvanostatic charge/discharge curves at a current density of 0.5 A/g; (c) Specific capacitance comparison as function of deposit loading amount; (d) Nyquist plots; (e) Bode plots; (f) Relative specific capacitance retention as function of scan rates.

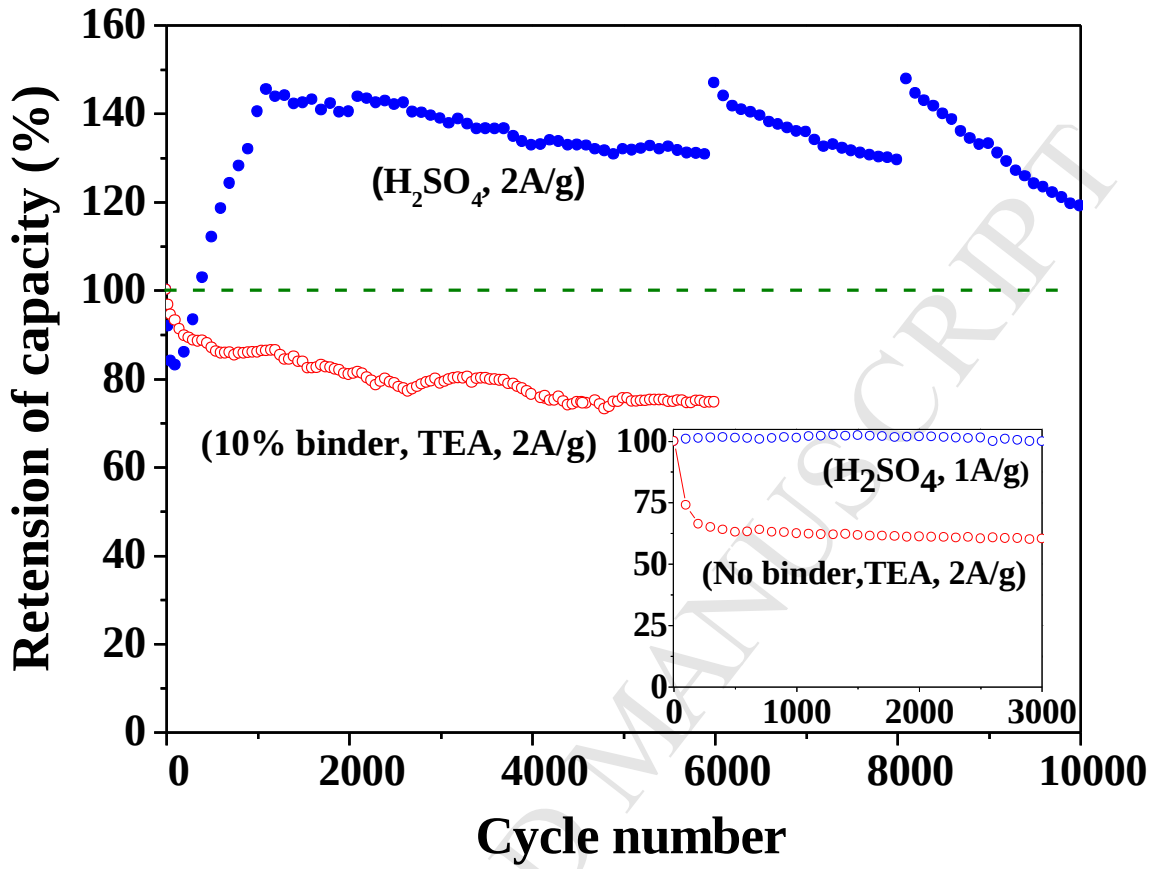

Fig. 6. Cycling stability performance of nano-DDDC-rGO electrodes measured at various conditions (e.g. aqueous vs. organic electrolyte, and binder effect)

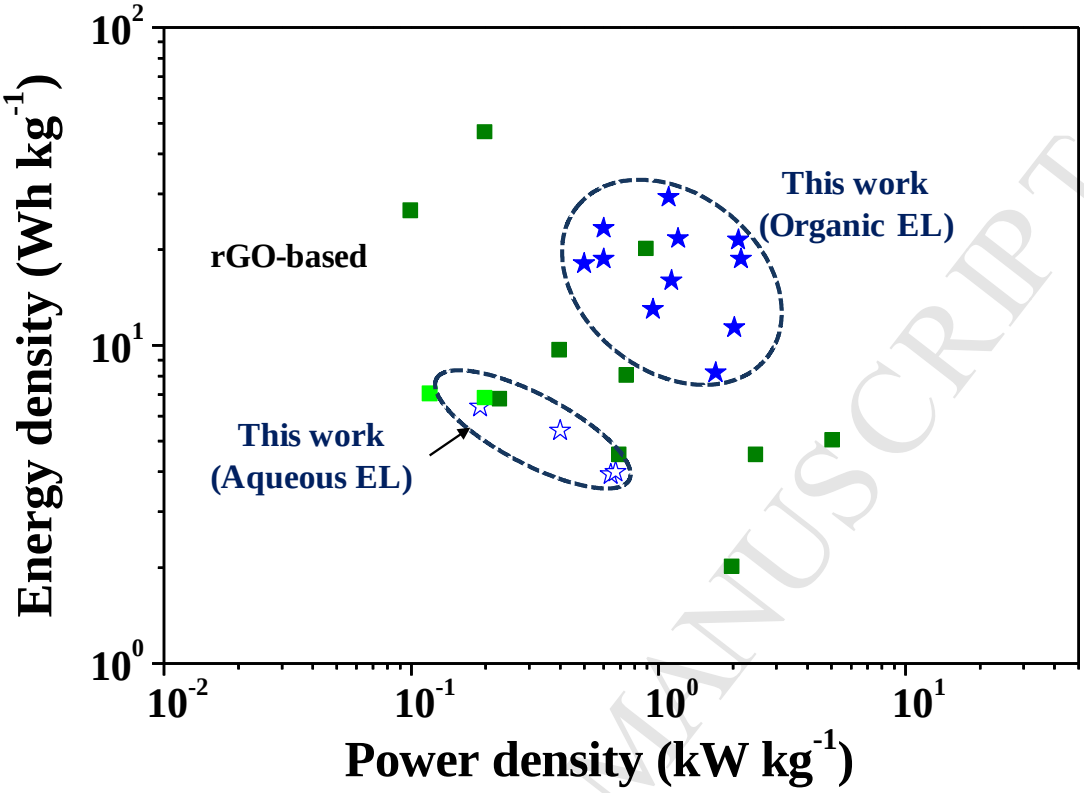

Fig. 7. Ragone plots of nano-DDDC-rGO supercapacitor. The values of other reported graphene based EDLC supercapacitors (i.e. symmetric cell) are added for comparison[4,5,6,7,10,1415,23]

Conflict of interest: The authors declare no completing financial interest

Supporting Information

Supporting Information is available from the Wiley Online Library or from the author.

Acknowledgements

This research work was supported by the Advanced Research Project Agency-Energy (ARPA-E) Program # DE-AR0000303. Part of the materials characterization (including XRD and SEM) was conducted at the Center for Nanophase Materials Sciences, which is sponsored by the ORNL Scientific User Facilities Division and DOE Office of Basic Research Sciences. The graphene coating deposition methods is also partially sponsored by the DOE/BETO program due to interest in graphene coated membrane development and applications

1 **References**
2

[1] F. Béguin, V. Presser, A. Balducci, E Frackowiak, Carbons and Electrolytes for Advanced Supercapacitors, Adv. Mater. 26 (2014) 2219-2251.

[2] K.S. Novoselov, V.I. Fal'ko, P.R. Gellert, M.G. Schwab, K. Kim, A rodmap for graphene, Nature 490 (2012) 192-200.

[3] F. Bonaccorso, L. Colombo, Guihua Yu, M. Stoller, V. Tozzini, A.C. Ferrari, R.S. Ruoff, V. Pellegrini, Graphene, related two-dimensional crystals, and hybrid systems for energy conversion and storage, Science 347, 6217 (2015) 1246501.

[4] L. Li, B. Song, L. Maurer, Z. Lin, G. Lian, C.C. Tuan, K.S. Moon, C.P. Wong, Molecular Engineering of Aromatic Amine Spacers for High-Performance Graphene-Based Supercapacitors, Nano Energy 21 (2016) 276-294.

[5] X. Lu, L. Li, B. Song, K.S. Moon, N. Hu, G. Liao, T. Shi, C.P. Wong, Mechanistic investigation of the graphene functionalization using p-phenylenediamine and its application for supercapacitors, Nano Energy 17 (2015) 160-170.

[6] B. Song, C. Sizemore, L. Li, X. Huang, Z. Lin, K.S. Moon, C.P. Wong, Triethanolamine functionalized graphene-based composites for high performance supercapacitors, J. Mater. Chem. A. 3 (2015) 21789-21796.

[7] J.H. Lee, N. Park, B.G. Kim, D.S. Jung, K. Im, J. Hur, J.W. Choi, Restacking-Inhbited 3D Reduced Graphene Oxide for High Performance Supercapacitor Electrodes, ACS Nano 10 (2013) 9366-9374.

[8] B. Song, J.I. Choi, Y. Zhu, Z. Geng, L. Zhang, Z. Lin, C. Tuan, K.S. Moon, C.P. Wong, Molecular Level Study of Graphene Networks Functionalized with Phenylenediamine Monomers for Supercapacacitor Electrodes, Chem. Mater. 28 (2016) 9110-9121.

[9] B. Song, J. Zhao, M. Wang, J. Mullavey, Y. Zhu, Z. Geng, D. Chen, Y. Ding, K.S, Moon, M. Liu, C.P. Wong, Systematic study on structural and electronic properties of diamine/ triamine functionalized graphene networks for supercapacitor application, Nano Energy 31 (2017) 183-193.

[10] Y. Hwang, S.M. Lee, Y.J. Kim, Y.H. Kahng, K. Lee, A new approach of structural and chemical modification on graphene electrodes for high-performance supercapacitors, Carbon 100 (2016) 7-15.

[11] Y. Yoon, K. Lee, S. Kwon, S. Seo, H. Yoo, S. Kim, Y. Shin, Y. Park, D. Kim, J. Choi, H. Lee, Vertical Alignments of Graphene Sheets Spatially and Densely Piled for Fast Ion Diffusion in Compact Supercapacitors, ACS Nano 8 (2014) 4580-4590.

[12] Z. Bo, W. Zhu, W. Ma, Z. Wen, X. Shuai, J. Chen, J. Yan, Z. Wang, K. Cen, X. Feng, Vertically Oriented Graphene Bridging Active-Layer/Current-Collector interface for Ultrahigh Rate Supercapacitors, Adv. Mater. 25 (2013) 5799-5806.

[13] Z. Ling, Z. Wang, M. Zhang, C. Yu, G. Wang, Y. Dong, S. Liu, Y. Wang, J. Qiu, Sustainable Synthesis and Assembly of Biomass-Derived B/N Co-Doped Carbon Nanosheets with Ultrahigh Aspect Ratio for High-Performance Supercapacitors, Adv. Funct. Mater. 26 (2016) 111-119.

[14] J. Yan, Q. Wang, T. Wei, L. Jiang, M. Zhang, X. Jing, Z. Fan, Template-Assisted Low Temperature Synthesis of Functionalized Graphene for Ultrahigh Volumetric Performance Supercapacitors, ACS Nano 8 (2014) 4720-4729.

[15] V. Sahu, S. Shekhar, R. K. Sharma, G. Singh, Ultrahigh Performance Supercapacitor form Lacey Reduced Graphene Oxide Nanoribbons, ACS Appl. Mater. Interfaces 7 (2015) 3110-3116.

[16] S. Li, C. Yu, J. Yang, C. Zhao, X. Fan, H. Huang, X. Han, J. Wang, X. He, J. Qiu, Ultrathin Nitrogen-Enriched Hybrid Carbon Nanosheets for Supercapacitors with Ultrahigh Rate Performance and High Energy Density, ChemElectroChem 4 (2017) 369-375.

[17] Y. Lin, X. Han, C. J. Campbell, J. Kim, B. Zhao, W. Luo, J. Dai, L. Hu, J.W. Connell, Holey Graphene Nanomanufacturing: Structure, Composition, and Electrochemical Properties, Adv. Funct. Mater. 25 (2015) 2920-2927.

[18] Z. Li, H. Zhang, Q. Liu, Y. Liu, L. Stanciu, J. Xie, Covalently-grafted polyaniline on graphene oxide sheets for high performance electrochemical supercapacitors, Carbon 71 (2014) 257-267.

[19] D.C. Marcano, D.V. Kosynkin, J.M. Berlin, A. Sinitskii, Z. Sun, A. Slesarev, L.B. Alemany, W. Lu, J.M. Tour, Improved Synthesis of Graphene Oxide, ACS nano, 4 (2010) 4806-4814.

[20] G. G. Jang, Jong K. Keum, B. Song, L. Li, Y. Jiang, A. Hunt, K.-S. Moon, C. P. Wong, M. Z. Hu, Microscopic Vertical Orientation of Nano-Interspaced Graphene Oxide Architectures in Deposit Films as Electrodes for Enhanced Supercapacitor Performance, Nano Energy 32 (2017) 88-95.

[21] L.L. Zhang, X. Zhao, M.D. Stoller, Y. Zhu, H. Ji, S. Murali, Y. Wu, S. Perales, B. Clevenger, R.S. Ruoff, Highly Conductive and Porus Activated Reduced Graphene oxide Films for High-Power Supercapactiors, Nano Lett. 12 (2012) 1806-1821.

[22] J.R, Miller, R.A. Outlaw, B.C. Holloway, Graphene Dobule-Layer Capacitor with ac Line-Filtering Performance, Science 329 (2010) 1637-1639.

[23] W. Ai, W. Zhou, Z. Du, Y. Du, H. Zhang, X. Jia, L. Xie, M. Yi, T. Yu, W. Huang, Benzoxazole and benzimidazole heterocycle-grafted graphene for high-performance supercapacitor electrodes, J. Mater. Chem., 22 (2012) 23439-23446.